Journal of Biomolecular NMR **29:** 11–20, 2004.

Dipolar assisted rotational resonance NMR of tryptophan and tyrosine in rhodopsin

Evan Crocker[a], Ashish B. Patel[b], Markus Eilers[c], Shobini Jayaraman[e], Elena Getmanova[d], Philip J. Reeves[d], Martine Ziliox[c], H. Gobind Khorana[d], Mordechai Sheves[e] & Steven O. Smith[c]

Departments of [a]*Physics and Astronomy,* [b]*Physiology and Biophysics,* [c]*Biochemistry and Cell Biology, Center for Structural Biology, SUNY at Stony Brook, Stony Brook, NY 11794-5115, U.S.A.;* [d]*Department of Biology, Massachusetts Institute of Technology, Cambridge, MA 02139, U.S.A.;* [e]*Department of Organic Chemistry, Weizmann Institute of Science, Rehovot, Israel*

Received 29 July 2003; Accepted 3 December 2003

Key words: DARR, dipolar assisted rotational resonance; GPCR, G protein-coupled receptor; MAS, magic angle spinning; NMR, nuclear magnetic resonance; PDSD, proton-driven spin diffusion; REDOR, rotational echo double resonance; RFDR, radiofrequency driven recoupling; TM, transmembrane; VACP, variable amplitude cross polarization

Abstract

Two dimensional (2D) solid-state ^{13}C...^{13}C dipolar recoupling experiments are performed on a series of model compounds and on the visual pigment rhodopsin to establish the most effective method for long range distance measurements in reconstituted membrane proteins. The effects of uniform labeling, inhomogeneous B_1 fields, relaxation and dipolar truncation on cross peak intensity are investigated through NMR measurements of simple amino acid and peptide model compounds. We first show that dipolar assisted rotational resonance (DARR) is more effective than RFDR in recoupling long-range dipolar interactions in these model systems. We then use DARR to establish ^{13}C-^{13}C correlations in rhodopsin. In rhodopsin containing 4′-^{13}C-Tyr and 8,19-^{13}C retinal, we observe two distinct tyrosine-to-retinal correlations in the DARR spectrum. The most intense cross peak arises from a correlation between Tyr268 and the retinal 19-$^{13}CH_3$, which are 4.8 Å apart in the rhodopsin crystal structure. A second cross peak arises from a correlation between Tyr191 and the retinal 19-$^{13}CH_3$, which are 5.5 Å apart in the crystal structure. These data demonstrate that long range ^{13}C...^{13}C correlations can be obtained in non-crystalline integral membrane proteins reconstituted into lipid membranes containing less than 150 nmoles of protein. In rhodopsin containing 2-^{13}C Gly121 and U-^{13}C Trp265, we do not observe a Trp-Gly cross peak in the DARR spectrum despite their close proximity (3.6 Å) in the crystal structure. Based on model compounds, the absence of a ^{13}C...^{13}C cross peak is due to loss of intensity in the diagonal Trp resonances rather than to dipolar truncation.

Introduction

The visual photoreceptor rhodopsin is a member of the family of G protein-coupled receptors (GPCRs) (Menon et al., 2001). These receptors have a common architecture consisting of seven transmembrane helices. Activation of rhodopsin by light is initiated by isomerization of the photoreactive 11-*cis* retinylidene chromophore. The chromophore is covalently bound within the bundle of transmembrane helices through a protonated Schiff's base linkage to Lys296. Despite intensive biochemical efforts, the mechanism for how retinal isomerization is coupled to receptor activation has yet to be determined. The crystal structure of rhodopsin in the dark, inactive state has been solved to high resolution (Okada et al., 2002; Palczewski

*To whom correspondence should be addressed. E-mail: steven.o.smith@sunysb.edu

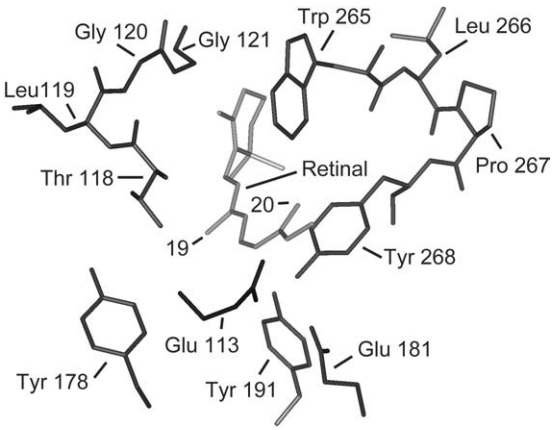

Figure 1. Structure of the retinal binding pocket in rhodopsin. The retinal is gray and the amino acids are black. Thr118 through Gly121 constitute a turn of TM helix 3 and Trp265 through Tyr268 constitute a turn of TM helix 6. Glu113 is the counterion to the protonated Schiff's base. Tyr178, Tyr191, and Glu181 are all on the extracellular loop between TM helices 4 and 5, which caps the extracellular side of the binding pocket.

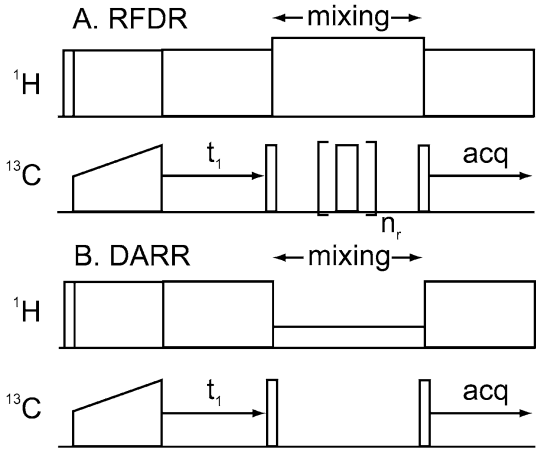

Figure 2. Pulse sequences for the RFDR (A) and DARR (B) experiments. Both sequences begin with VACP using a ramped pulse on the ^{13}C channel. After the evolution period, magnetization is placed along the z-axis with a 90° pulse and mixing occurs longitudinally with either a high power ^{1}H decoupling pulse in RFDR or a low power ^{1}H 'recoupling' pulse in DARR. During the DARR mixing period, the ^{1}H RF field strength is set to the $n = 1$ rotational resonance condition. In the RFDR experiment, mixing is driven by a train of rotor synchronized 180° pulses on the ^{13}C channel. Two pulse phase modulated decoupling is used during acquisition and evolution.

et al., 2000). However, the conformational changes that occur upon light-activation crack the rhodopsin crystals, preventing the determination of a structure of the activated receptor by protein crystallography.

The retinal chromophore is the trigger for rhodopsin activation. Figure 1 shows the retinal binding site from the rhodopsin crystal structure and highlights several of the key amino acids that surround the retinal. These residues are located primarily on transmembrane (TM) helices 3 and 6, and are essential for activation. Moreover, they are conserved throughout the rhodopsin class of GPCRs. One of the most highly conserved residue in GPCRs is Pro267 on TM helix 6. In addition, the two aromatic residues, Trp265 and Tyr268, which bracket Pro267, are highly conserved in all visual pigments. Mutation of Trp265, Tyr268 or Pro267 results in loss of activity (Nakayama and Khorana, 1991). TM helix 3 also contains several conserved and critical amino acids. Glu113 serves as the counterion for the protonated retinal Schiff's base (Jager et al., 1994) and mutation to Gln results in constitutive receptor activity (Robinson et al., 1992). Gly121 is strictly conserved in the visual pigments. Substitution of Gly121 with amino acids having larger side chains results in receptor activation in the dark (Han et al., 1996). The current consensus for the activation mechanism is that retinal isomerization triggers rigid body motion of TM helices 3 and 6 (Farrens et al., 1996). However, the mechanism for how retinal isomerization is coupled to helix motion via interactions with the neighboring residues in the retinal binding pocket is not known.

Solid-state NMR provides a way to establish the key structural changes occurring upon receptor activation. Long-range ^{13}C…^{13}C and ^{13}C…^{15}N distance measurements yield structural constraints if unique isotope labels can be incorporated into the protein. Isotope labeling of the retinal has been used extensively to investigate the structure of the chromophore (Smith et al., 1990; Creemers et al., 2002) and we have shown that isotope labels can be incorporated into amino acids of the protein by expressing rhodopsin in HEK293S cells using labeled growth media (Eilers et al., 1999). The question is whether isotope labeling of the retinal and protein can be combined to obtain distance constraints within the binding pocket of rhodopsin. The challenge is that rhodopsin is non-crystalline and is inherently at low concentration (<200 nmoles of total protein) when reconstituted into lipid membranes.

A wide range of methods has been developed over the past 15 years for measuring dipolar couplings in solid state magic angle spinning (MAS) experiments. However, in contrast to solution state NMR, there is no established suite of solid-state NMR experiments for membrane protein structure determination. One-

dimensional recoupling techniques, such as rotational resonance (Raleigh et al., 1988) and REDOR (Gullion and Schaefer, 1989), have been used widely to obtain distances between isolated pairs of labels. The efficacy of these methods is hindered by two problems associated with solid state NMR of membrane proteins: broad lines due to the non-crystalline nature of the sample and a large natural abundance background signal from the reconstituted membrane. In these cases, one must rely on isotope labeling of sites in proteins with unique chemical shifts in order to obtain the resolution necessary to make precise and accurate measurements. 2D techniques that form the basis of chemical shift resolution in multidimensional solution NMR have not been as extensively applied for structural studies of membrane proteins by solid-state NMR. There are two problems associated with two-dimensional methods in biological solid-state NMR. One is the loss of signal due to the dephasing of magnetization by inhomogeneous B_1 fields. The other is dipolar truncation, where a weak correlation between two spins is not observed if one or both of these spins is also strongly dipolar coupled to other spins.

In this paper, we first compare dipolar assisted rotational resonance (DARR), a recently developed extension of the proton-driven spin diffusion (PDSD) experiment, to radio frequency driven recoupling (RFDR) for measuring $^{13}C\ldots{}^{13}C$ through space correlations (Takegoshi et al., 2001). The RFDR sequence (Bennett et al., 1998) has been extensively used for characterizing directly bonded ^{13}C-^{13}C correlations (Sodickson et al., 1993), and has been applied to measure long range $^{13}C\ldots{}^{13}C$ correlations in the membrane protein bacteriorhodopsin (Griffiths et al., 2000). Using a series of model compounds, we demonstrate that the DARR experiment is more effective than RFDR at measuring the long range, through-space correlations that carry the most information concerning structure. We also show that DARR is less sensitive to inhomogeneous B_1 fields than RFDR, allowing one to use the full volume of the MAS rotor when the sample concentration is low.

In the standard solid state 2D correlation experiments, dipolar truncation prevents the measurement of the weak dipolar couplings of interest in the presence of strong couplings from directly bonded ^{13}C (Schmidt-Rohr and Spiess, 1994). This effect is arguably the most significant problem for structural studies of membrane proteins. In many cases, the use of uniformly labeled amino acids would be a significant advantage, either due to the lack of readily attainable singly labeled amino acids or the additional information a uniformly labeled sample would bring. The DARR sequence has been reported to solve problems associated with dipolar truncation (Takegoshi et al., 2001). Using phenylalanine methyl ester that has been uniformly ^{13}C labeled in the aromatic ring and singly ^{13}C labeled at the methyl ester, we determine the effects of dipolar truncation on DARR in the measurement of a weak aromatic – methyl correlation. This is an appropriate model system for rhodopsin because aromatic amino acids are prevalent in the retinal binding site of rhodopsin and the retinal methyl groups are thought to be part of the steric trigger in the activation mechanism.

We illustrate the advantages of DARR on rhodopsin containing ^{13}C-labeled amino acids and ^{13}C-labeled retinal. We have focused on the amino acids tyrosine, tryptophan and glycine that form part of the retinal binding site. The 4′-^{13}C Tyr rhodopsin sample was regenerated with 8,19-^{13}C retinal. The 2.5 Å separation between the 8-^{13}C and 19-^{13}C labels on the retinal provides a known internal distance for calibrating protein-retinal measurements. In the crystal structure of rhodopsin, the closest tyrosine to the retinal 19-$^{13}CH_3$ group is Tyr268 on TM helix 6. We show that the 4.8 Å distance between the retinal and Tyr268 can be detected using DARR, but not RFDR. The distance range of the DARR method is reflected in the observation of a distinct cross peak that arises from Tyr191 which is 5.5 Å from the 19-$^{13}CH_3$ group. These studies provide the foundation for studying the structure of the activated metarhodopsin II intermediate and other membrane proteins that contain ^{13}C-labeled amino acids.

Materials and methods

Synthesis and preparation of AGG model compounds

Alanyl glycylglycine (AGG) model peptides were synthesized using fMOC chemistry at the W.M. Keck facility at Yale University, and purified by reverse phase-HPLC and recrystallization. The ^{13}C-labeled AGG peptide was diluted 1:10 with unlabeled peptide to minimize intermolecular $^{13}C\ldots{}^{13}C$ couplings.

Uniform-^{13}C-ring, ^{13}C-methyl phenylalanine methyl ester was made by the following procedure. First, acetyl chloride (150 μl) was slowly added dropwise into 1 ml of ^{13}C-methanol on ice. ^{13}C-ring labeled phenylalanine (40 mg) was then slowly added and the

solution was incubated at 30 °C for 6 h. After incubation, the solution was evaporated by argon and lyophilized overnight. The purity of the final product was confirmed to be >95% by mass spectroscopy.

Expression of labeled rhodopsin

Bovine rhodopsin was expressed in mammalian HEK293S cells adapted for suspension growth. Details of the expression protocols and the cell media have been described elsewhere (Reeves et al., 1999). Briefly, HEK293S cells containing a tetracycline inducible rhodopsin gene were used (Reeves et al., 2002). Cells were grown to confluence on 15 cm cell culture dishes. 8 dishes per liter were used to inoculate a 10L New Brunswick Scientific Celligen Plus bioreactor containing 4 l of media, prepared with 72.5 mg/l (0.4 mM) of 4′-^{13}C labeled Tyr or 16 mg/l (0.08 mM) of U-^{13}C Trp and 30 mg/l (0.4 mM) of 2-^{13}C Gly. Induction of gene expression was by tetracycline and sodium butyrate addition, and was initiated 4 days after inoculation. An additional feeding of the cells with glucose and salts was done 2 days prior to harvesting.

Purification of rhodopsin

HEK293S cells were harvested and treated with unlabeled 11-*cis* retinal to regenerate rhodopsin. The cells were next solubilized in 1.5% (w/v) octyl β-glucoside, 50 mM NaCl, 10 mM Na_2HPO_4, pH 6 for 4 h. Purification of rhodopsin was by Sepharose rho-1D4 antibody chromatography. Rhodopsin was obtained at 1 mg/ml after elution and concentration by Amicon centrifugation devices. Purified rhodopsin was subsequently suspended in prepared 75% DOPE/25% DOPC liposomes at a 1:100 protein:lipid ratio. 50 fold dialysis was used to remove all detergent, and the resulting proteoliposomes were pelleted and frozen at −80 °C.

Synthesis of 8,19-^{13}C retinal

Citral was condensed in methanol with 1 equivalent of 1,3-$^{13}C_2$ acetone in the presence of NaOH at 25 °C for 30 min. The product was cyclized to β-ionone with H_2SO_4 in nitromethane at 0 °C for 15 min. The labeled β-ionone was converted to 8,19-^{13}C retinal by a Horner–Emmons reaction with diethyl phosphonoacetonitrile followed by reduction with diisobutyl aluminium hydride (DIBAL). Condensation with diethyl-(3-carbonitrile-2-methyl-2-propenyl) phosphonate and reduction with DIBAL yielded the labeled retinal. The 11-*cis* isomer was purified by HPLC following irradiation of the all-trans retinal in acetonitrile. The mixture of isomers was purified on a 10 μm Alltech Econosphere normal phase silica column using a 96% hexane, 4% ethyl acetate solvent mixture at a flow rate of 8 ml/min. $CaCl_2$ pellets were added to the solvent overnight to remove all water and the solvent was filtered prior to use. During purification, helium was bubbled through the solvent to remove dissolved gases.

Regeneration of rhodopsin with labeled retinal

Rhodopsin (5 mg in 1 ml) was bleached using a 400 W projector lamp with a >495 nm cutoff filter for 30 s. 8,19-^{13}C 11-*cis* retinal was added at a 2:1 molar excess of retinal to opsin and the rhodopsin pigment was regenerated by end-over-end mixing overnight at room temperature.

NMR spectroscopy

Experiments were carried out on Bruker NMR spectrometers at either a 360 or 600 MHz ^{1}H frequency using Bruker 4 mm MAS probes. MAS speeds for all experiments were maintained at 13 kHz +/− 5 Hz by a Bruker MAS controller unit, except for the experiments on phenylalanine methyl ester which were run at 9 kHz. Rhodopsin experiments were carried out at −70 °C to −80 °C.

Variable amplitude cross polarization (VACP) (Peersen et al., 1994) contact times were 2 ms in all experiments and two pulse phase modulated (Bennett et al., 1995) decoupling was used during the evolution and acquisition periods. As the 1:3 power mismatch ratio suggested by Sodickson et al. (Sodickson et al., 1993) could not be maintained throughout the entire mixing period of the RFDR experiment due to hardware limitations, the ^{1}H power was increased during the ^{13}C 180° mixing pulses in order to reach the suggested power mismatch. During the mixing period of the DARR experiment, the ^{1}H RF field strength was set to the frequency corresponding to the $n = 1$ rotational resonance condition (Takegoshi et al., 2003).

The RFDR sequence recouples the homonuclear dipolar interaction through a train of rotor synchronized 180° pulses on the observe nucleus (Figure 2). The pulse train reintroduces the zero quantum (flip-flop) part of the dipolar coupling term of the spin Hamiltonian, allowing for magnetization exchange between coupled spins. The magnetization exchange

rate is relatively rapid and the sequence requires only standard pulse lengths (90° and 180° pulses) and phases (x, −x, y, −y). There are, however, several drawbacks to RFDR. First, refocusing of the magnetization for acquisition is sensitive to precise setting of the 180° pulse lengths. As a result, B_1 inhomogeneity causes significant dephasing of the signal when the sample is not constrained to the center of the rotor. This is a problem for membrane protein samples for which we typically use the full volume of the MAS rotor in order to enhance sensitivity. Second, to get efficient magnetization transfer, the fields on the observe and decoupling channels must be mismatched by at least a 1:3 ratio in order to prevent unwanted cross polarization during mixing. The length of the mixing time, and therefore the maximum observable distance, is limited by the capabilities of the hardware due to this requirement for high ^{1}H power.

Dipolar assisted rotational resonance (DARR) uses a combination of mechanical rotation of the sample and the ^{13}C-^{1}H dipolar interaction to reintroduce the homonuclear dipolar coupling (Takegoshi et al., 2001). As in rotational resonance (Raleigh et al., 1988), magnetization is exchanged when a spinning sideband of one spin overlaps with the isotropic resonance or sideband of another. Irradiation of the protons at the rotational resonance condition efficiently recouples the ^{13}C-^{1}H dipolar interaction, broadening the lines in the carbon spectrum. This broadening relaxes the discrete rotational resonance condition by increasing the frequency range over which two lines will overlap. The absence of pulses during the mixing period on the observe channel frees this experiment from the problems seen in RFDR.

Results and discussion

Comparison of DARR and RFDR in AGG and Amino Acid Model Compounds

We first compare RFDR and DARR for measuring ^{13}C correlations in the tripeptide AGG that has been ^{13}C-labeled at the methyl carbon of Ala1 and the carbonyl carbon of Gly2. The structure of AGG is known (Subramanian and Lalitha, 1983) and the labeling scheme produces an isolated spin pair separated by 4.6 Å. In both RFDR and DARR, the ^{13}C-labels yield intense resonances along the diagonal of the 2D spectrum and the weak (78 Hz) dipolar coupling between the two labels gives rise to an off diagonal cross peak. The intensity of the cross peak and the rate at which it builds

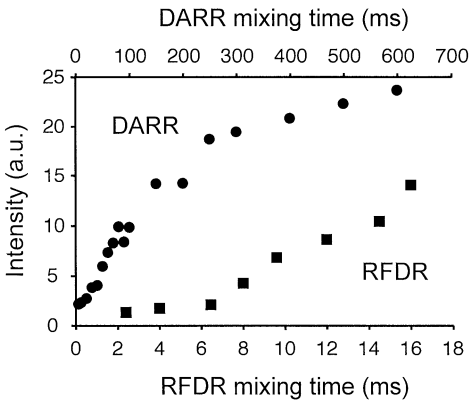

Figure 3. Buildup of cross peak intensity in 1-^{13}C-Ala, 2-^{13}C-Gly labeled AGG using DARR (circles) and RFDR (squares). Note the different timescales of the two experiments. The ^{13}C...^{13}C distance in 2-^{13}C-Ala1, 1-^{13}C-Gly2 is 4.6 Å based on the crystal structure of AGG. All experiments were performed with 16 scans and 256 t_1 increments. Intensity values are arbitrary.

up during the mixing period reflects the strength of the ^{13}C...^{13}C dipolar coupling. Figure 3 presents the buildup curves of cross peak intensity as a function of the mixing time. Note that the range of mixing times used is different for RFDR and DARR. The maximum mixing time for the RFDR experiment is limited to 16 ms in order to avoid probe breakdown due to the high power required on the proton channel during the mixing period. On the other hand, the DARR sequence is not subject to such hardware limitations, as it has no pulses on the observe channel and only low power on the ^{1}H channel during the mixing period. In the DARR experiment, mixing times up to 1–2 s are possible.

The cross peak buildup curves in Figure 3 show the differences between DARR and RFDR. In RFDR, the cross peak intensity builds up rapidly during the 16 ms mixing time and reaches a value of 15 (see figure legend), which is significantly greater than the intensity in the DARR experiment with 16 ms of mixing. However, due to the hardware limitations discussed above the mixing time in the RFDR experiment is not increased beyond 16 ms. In contrast, longer mixing times can be used for DARR, and after 200 ms the intensity of the DARR cross peak exceeds the maximum intensity attained by RFDR. These data show that for a simple system with two weakly coupled, isolated ^{13}C spins, the longer mixing times possible with DARR provide significant advantages over RFDR.

In contrast to AGG above, tryptophan, an aromatic amino acid found in the retinal binding site of rhodopsin, has a strongly coupled network of spins when

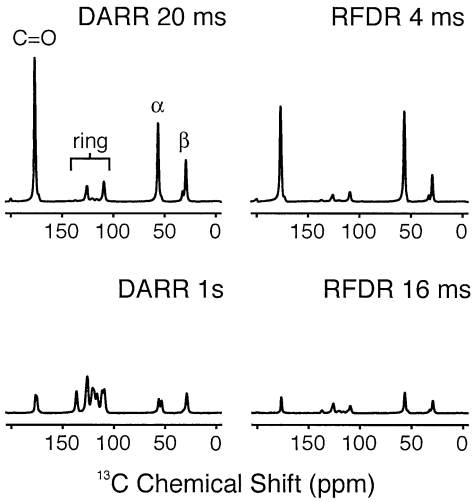

Figure 4. Comparison of cross peak intensities in U-^{13}C tryptophan using RFDR (right column) and DARR (left column). The 1D spectra correspond to rows from a 2D experiment taken through the carbonyl diagonal peak. RFDR mixing times are 4 ms (above) and 16 ms (below). DARR mixing times are 20 ms (above) and 1 s (below). The peak at 176 ppm is the carbonyl diagonal peak. Data were acquired with 256 t_1 increments and spinning at 13 kHz.

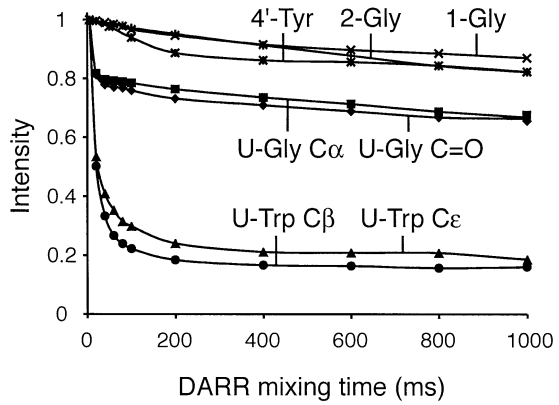

Figure 5. Comparison of diagonal peak intensity as a function of the DARR mixing time for a series of model compounds. The decay of the diagonal peak intensity is less than 10% for singly ^{13}C labeled amino acids (1-^{13}C-Gly, 2-^{13}C-Gly, 4′-^{13}C-Tyr). The decay increases for the carbonyl and α-carbons of U-^{13}C-Gly, and the α- and ε-carbons of U-^{13}C-Trp as a function of mixing time. All diagonal signals are normalized to 1 at 5 ms of mixing. Lines are drawn to guide the eye.

uniformly ^{13}C-labeled. Figure 4 compares the cross peak and diagonal peak intensity in 2D DARR and RFDR spectra of U-^{13}C-Trp. Each spectrum in Figure 4 corresponds to a row from a 2D experiment taken through the carbonyl diagonal peak. The carbonyl diagonal peak is observed at 177 ppm, and exhibits cross peaks to the β-carbon at 29 ppm, the α-carbon at 55 ppm and the aromatic ring carbons between 106 and 139 ppm. At the short mixing times for the two experiments, buildup of cross peak intensity is rapid and essentially complete for the strongly coupled (e.g. directly bonded) spins. Strong cross peaks are observed to the α and β carbons due to their close proximity to the carbonyl carbon. Weak cross peaks are observed for the aromatic ring carbons, which are farther away from the carbonyl. At longer mixing times in both experiments, the cross peak intensity decreases due to the overall decay of the signal (see below). However, the cross peak intensity of the aromatic ring carbons is still growing at longer mixing times in the DARR experiment. Magnetization exchange via spin diffusion through the network of tightly coupled spins accounts for the growing intensity observed in carbons that are spatially distant from the carbonyl.

Figure 5 illustrates how the diagonal peak intensity decreases in DARR as a function of mixing time for several different amino acid model compounds. For amino acids with single, isolated ^{13}C labels (1-^{13}C Gly, 2-^{13}C Gly, and 4′-^{13}C Tyr), the intensity of the diagonal resonance only decreases about 10% over the course of the mixing time series due to T_1 relaxation. Of note is that the size of the chemical shift anisotropy (CSA) does not influence the intensity of the diagonal signal. In contrast, the intensity of the diagonal resonances in U-^{13}C Gly decreases by about 20% within the first 20 ms of mixing as a result of the strong homonuclear dipolar coupling that is reintroduced. A much more dramatic loss of diagonal peak intensity is observed in U-^{13}C Trp, which has a large network of tightly coupled ^{13}C nuclei. The same loss of diagonal intensity is observed at 16 ms of mixing in the RFDR experiment for U-^{13}C Trp (Figure 4). Such losses of intensity represent a drawback of 2D homonuclear recoupling experiments on uniformly labeled samples and likely result from equilibration of ^{13}C polarization between all of the directly bond carbons. This is reflected in the relatively uniform intensities of the carbon resonances in the DARR spectrum of U-^{13}C-Trp in Figure 4 obtained with a mixing time of 1 s.

The effect of inhomogeneous B_1 fields on the signal intensity in the DARR and RFDR spectra is shown in Figure 6. In simple solenoid coils, the B_1 field is strongest at the center of the coil and decreases toward the ends. This results in different pulse flip angles for a given pulse length in different regions of the NMR rotor. Figure 6A is the 1D spectrum of U-^{13}C-Trp constrained to the bottom third of a 4 mm NMR rotor obtained with variable amplitude cross

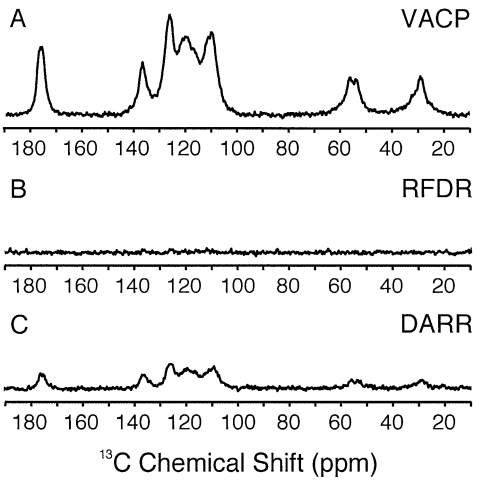

Figure 6. Effects of inhomogeneous B_1 fields in U-^{13}C tryptophan. The sample was constrained to the bottom third of the rotor, and 1D spectra were obtained with VACP (A), RFDR (B) and DARR (C).

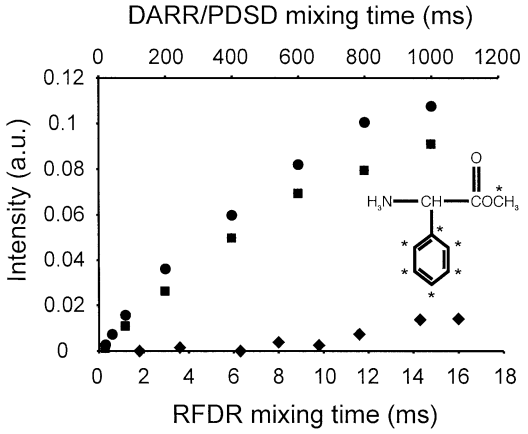

Figure 7. Cross peak buildup in phenylalanine methyl ester using DARR (circles), PDSD (squares) and RFDR (diamonds). The sample was uniformly ^{13}C-labeled in the aromatic ring and singly ^{13}C-labeled in the methyl group of the methyl ester. Cross peak intensities are normalized to the diagonal peak intensities. Note the different timescales of the experiments. Data were acquired with 64 t_1 increments and spinning at 9 kHz. Inset: Structure of phenylalanine methyl ester with ^{13}C labels marked with asterisks.

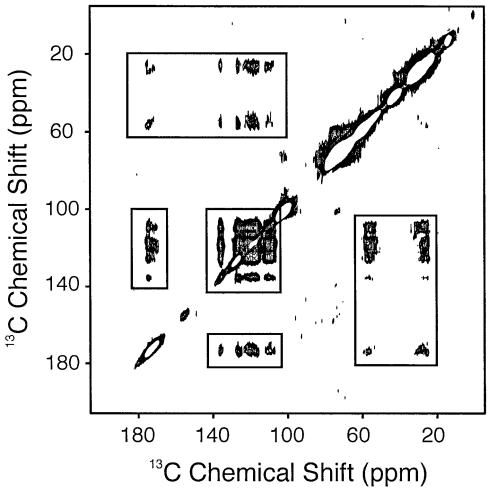

Figure 8. Two-dimensional DARR spectrum of 2-^{13}C Gly, U-^{13}C Trp rhodopsin obtained with 500 ms of mixing. The boxed cross peaks arise from intramolecular couplings within individual tryptophan residues. Data were acquired with 128 t_1 increments and spinning at 13 kHz.

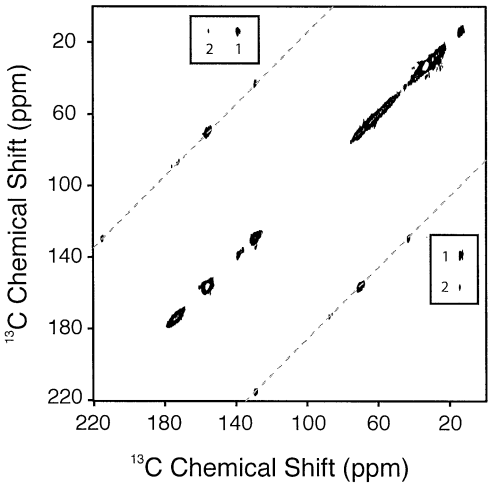

Figure 9. Two-dimensional DARR spectrum of 4′-^{13}C-Tyr-labeled regenerated with 8,19-^{13}C retinal. The cross peaks denoted by 1 arise from the 8-^{13}C...19-^{13}C dipolar coupling and the cross peaks denoted by 2 arise from the 4′-^{13}C-tyrosine...19-^{13}C-retinal dipolar coupling. Data were acquired with 64 t_1 increments and spinning at 13 kHz. The dashed line indicates cross peaks resulting from spinning side bands.

polarization (VACP). Ramping the amplitude of the CP pulse compensates for B_1 field inhomogeneity and substantially increases ^{13}C intensity at the end of the rotor. Figures 6B and C are a 1D RFDR experiment at 16 ms of mixing and a 1D DARR experiment at 1 s of mixing, respectively. In both DARR and RFDR, the magnetization is prepared with VACP providing the carbons with substantial magnetization before the mixing period, as shown in Figure 6A. While there is a significant amount of signal left after 1 s in the DARR spectrum, no signal can be seen after 16 ms in the RFDR spectrum. After the initial preparation and identical evolution periods, both sequences use a 90° pulse to flip the magnetization back to the longitudinal axis (Figure 2). As no other RF pulses are applied to the observe channel until the 90° read out pulse at the end of the mixing period, the effect of B_1 field

inhomogeneity is independent of the mixing time for the DARR experiment. On the other hand, the RFDR mixing sequence makes use of a train of 180° pulses on the observe channel. As the pulses were optimized on a sample centered in the coil, the pulse length does not correspond to a 180° flip angle for a sample constrained to the end of the coil. These improperly set pulses dephase the magnetization. Since the number of pulses increases with mixing time, the effect of B_1 field inhomogeneity also increases with mixing time. This will make the observation of weak couplings in samples filling the entire MAS rotor volume more difficult.

Finally, to evaluate the effects of dipolar truncation on both methods, we apply RFDR and DARR to phenylalanine methyl ester that has been ^{13}C-labeled at the aromatic Phe ring and at the methyl group of the methyl ester. In both cases, the sample was spun at 9 kHz in a 360 MHz ^{1}H field. DARR has been shown to give good correlations between all carbons in uniformly ^{13}C,^{15}N-labeled glycylisoleucine (Takegoshi et al., 2001), where dipolar truncation may affect the observation of weak, through space couplings. We use phenylalanine methyl ester to verify that a correlation can be seen between an isolated spin and a tightly coupled aromatic cluster. This is a good model for several cases that we would like to study in the binding pocket of rhodopsin, such as the distance between uniformly labeled Trp265 and singly labeled Gly121, or the position of the methyl groups of the retinal relative to the aromatic residues in the binding pocket. Depending on the dihedral angles separating the aromatic ring and the O-CH_3, the distances between the six ring carbons and the methyl carbon can range from 3.5 to 8.5 Å. Importantly, there are several ^{12}C atoms between the ^{13}C-labeled ring system and the ^{13}C-labeled methyl insuring that the magnetization exchange is not due to spin diffusion. In the ^{13}C,^{15}N-labeled glycylisoleucine dipeptide used by Takegoshi and coworkers, the ^{13}C networks of the glycine and isoleucine are only separated by two bonds (2.5 Å). ^{13}C-labeled phenylalanine methyl ester has been diluted 1:10 with unlabeled phenylalanine methyl ester in order to eliminate intermolecular correlations. As can be seen in Figure 7, there is significant magnetization exchange between the ring and the methyl group in the DARR experiment (circles). The cross peak intensity relative to the diagonal peak intensity is roughly equivalent to that seen in AGG. Even in the presence of stronger couplings, the correlation due to the weaker coupling can still be observed with DARR. In the RFDR experiment, even at the longest mixing time, the cross peaks have little intensity (diamonds).

For comparison, we also show the cross peak intensity between the aromatic ring and methyl carbons in the proton-driven spin diffusion (PDSD) experiment under the same experimental conditions (Figure 7, squares). The pulse sequence for PDSD is the same as for DARR but lacks the low power ^{1}H pulse during the mixing period. The cross peak intensity for PDSD is 15–20% less than for DARR at the longest mixing times. This is consistent with the comparison of DARR and PDSD by Takegoshi and colleagues on N-acetyl [1,2-^{13}C,^{15}N] DL-valine (Takegoshi et al., 2001; Takegoshi et al., 2003), defining DARR as the more efficient recoupling method.

DARR of 2-^{13}C Gly, U-^{13}C Trp-labeled rhodopsin

The 2D DARR spectrum of 2-^{13}C Gly, U-^{13}C Trp rhodopsin (Figure 8) was obtained on 100 nmoles (4 mg) of protein. The sample was spun at 13 kHz and 1536 scans were collected in each of 128 t_1 increments at a ^{1}H frequency of 360 MHz. There are 5 tryptophans and 23 glycines in rhodopsin, and the 2D spectrum is dominated by strong ^{13}C...^{13}C correlations from the U-^{13}C-labeled aromatic ring of tryptophan (boxed cross peaks). Although there is no chemical shift resolution of individual Trp or Gly amino acids along the diagonal, there is only one closely packed Trp-Gly pair in rhodopsin (Gly121 and Trp265), making any cross peak observed between these types of amino acids assignable to these specific residues. No cross peak is observed in the region corresponding to this pair. The Gly121-Trp265 distance in the crystal structure (3.6 Å) and the data collected on the phenylalanine methyl ester sample indicate that a correlation between these two residues is expected. The lack of an observed correlation is attributed to the rapid decay of Trp signal, as described above on model compounds, preventing the buildup of a visible cross peak.

DARR of 4′-^{13}C-Tyr-labeled rhodopsin

Rhodopsin contains 18 tyrosines, two of which are within 5.5 Å of the retinal. Figure 9 presents the 2D DARR spectrum of 150 nmoles (6 mg) 4′-^{13}C-Tyr-labeled rhodopsin regenerated with 8,19-^{13}C retinal. The sample was spun at 13 kHz and 3072 scans were collected in each of 64 t_1 increments at a ^{1}H frequency of 600 MHz. Incorporating the 8,19-^{13}C spin pair in the retinal has three advantages. First, observation of

the 8-^{13}C... 19-^{13}C cross peak, denoted as '1' in the boxed regions, provides an internal control showing that the rhodopsin is regenerated with labeled retinal. Second, the strong 8,19-^{13}C cross peaks allow us to accurately assign the chemical shifts of the 8-^{13}C and 19-^{13}C resonances in the 2D spectrum. This is important, particularly for the 19-^{13}C resonance, which is not resolved from the protein and lipid methyl resonances. Finally, the buildup of the 8-^{13}C... 19-^{13}C cross peak corresponds to a well-defined distance, giving an internal calibration for the experiment (as discussed below).

The cross peaks denoted with '2' in the boxed regions arise from the weaker 4′-^{13}C-tyrosine... 19-^{13}C-retinal coupling. According to the crystal structure, the distance between Tyr268 and 19-^{13}C of retinal is 4.8 Å (Palczewski et al., 2000). The weak coupling of the 19-$^{13}CH_3$ to 4′-^{13}C Tyr268 has a less intense cross peak than its stronger coupling to the 8-^{13}C of the retinal, as expected.

Figure 10 presents 1D slices through the 19-^{13}C retinal diagonal peak in 4-^{13}C-Tyr-labeled rhodopsin. Spectra were obtained with DARR mixing times of 200 ms (A), 1 s (B) and 1.5 s (C). There are three features to note in this series of spectra. The most intense peak in the three spectra is the cross peak between the 8-^{13}C and 19-^{13}C on the retinal. The peak is already intense with 200 ms of mixing, as expected from the short distance between the 8-^{13}C and 19-^{13}C labels. The peak at 155 ppm marked with an asterisk is assigned to Tyr268, which, according to the crystal structure, is in van der Waals contact with the retinal. A correlation between Tyr268 and the retinal would be the first tyrosine correlation to appear in a mixing time series. The Tyr268 peak occurs in the middle of the largely unresolved diagonal resonance corresponding to the 18 tyrosines in rhodopsin. The peak at 157 ppm, seen only in Figure 10C, is assigned to Tyr191, which is 5.5 Å from the retinal. As this coupling to the retinal is weaker, a longer mixing time is needed to observe the cross peak. The only other tyrosine within 10 Å of the 19-^{13}C methyl of the retinal is Tyr178 whose 4′-^{13}C carbon is 5.9 Å away. This distance appears to be outside of the detection range of the DARR experiment with our current sensitivity. These data illustrate that weak ^{13}C... ^{13}C dipolar couplings (i.e., long range distances) can be observed in the 2D DARR spectrum.

Figure 10D addresses the possibility of extracting quantitative distances from DARR cross peak intensities. Takegoshi et al. (2003) indicate that the cross peak

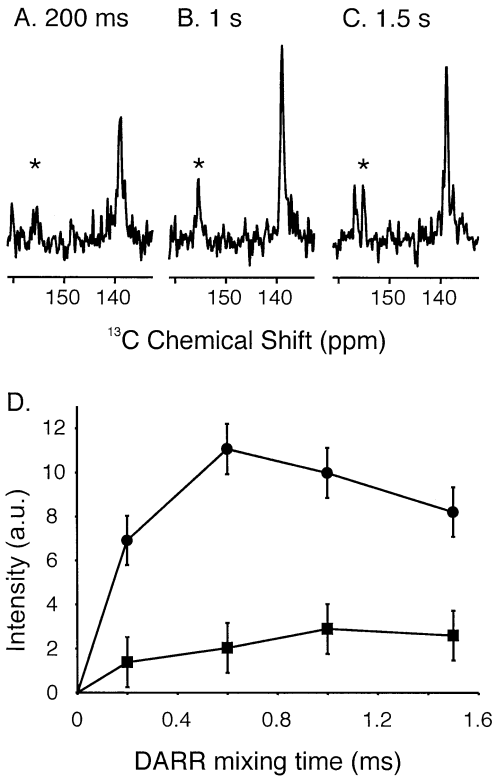

Figure 10. DARR cross peak intensities in rhodopsin. (A-C) One-dimensional slices through the 19-^{13}C retinal diagonal peak in 4-^{13}C-Tyr-labeled rhodopsin. Spectra were obtained with DARR mixing times of 200 ms, 1 s and 1.5 s. The peak at 155 ppm marked with an asterisk is the correlation between 4′-^{13}C-Tyr268 and the 19-^{13}C-methyl of retinal. (D) Cross peak intensity as a function of the DARR mixing time for the 8-^{13}C... 19-^{13}C-retinal correlation (circles, 2.5 Å) and the 4′-^{13}C-Tyr... 19-^{13}C-retinal correlation (squares, 4.8 Å).

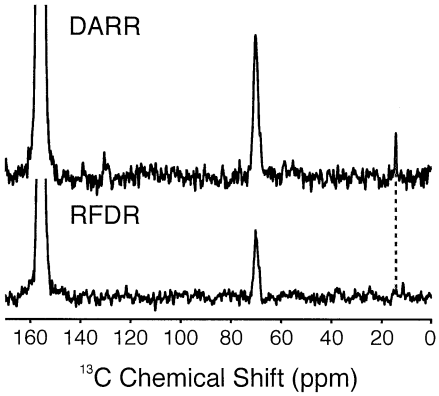

Figure 11. One-dimensional slices through the 4′-^{13}C tyrosine diagonal peak in 4-^{13}C-Tyr-labeled rhodopsin using DARR (upper trace) and RFDR (lower trace). The spectra were obtained with 1 s (DARR) and 16 ms (RFDR) mixing, and the position of the cross peak to the 19-^{13}C methyl carbon on the retinal is denoted by the dashed line.

intensities are influenced by several factors including homogeneous broadening due to ^{1}H-^{1}H dipolar interactions. The homogeneous ^{1}H-^{1}H interactions increase the efficiency of the DARR transfer, but are not easily simulated for complex spin systems. Nevertheless, there is a good qualitative agreement between cross peak intensities and internuclear distances in model compounds and in rhodopsin. Figure 10D presents the DARR cross peak build up curves for the 8-^{13}C... 19-^{13}C-retinal correlation and the 4′-^{13}C-Tyr... 19-^{13}C-retinal correlation. The intramolecular distance between the 8- and 19-^{13}C sites in retinal is 2.5 Å and fixed, while the 4.8 Å distance between the 4′-^{13}C-Tyr and 19-^{13}C retinal carbons is known from the crystal structure of rhodopsin. The curves show that both the rate at which cross peak intensity builds up and the maximum intensity of a cross peak are correlated to the strength of the dipolar coupling. The intramolecular retinal distance also provides an internal control for DARR measurements of rhodopsin intermediates where retinal-protein distances are not independently known.

Finally, Figure 11 shows the rows from 2D spectra taken through the tyrosine diagonal peak obtained using DARR at 1.5 s (above) and RFDR at 16 ms (below). In both cases, the sample was spun at 13 kHz and 3072 scans were collected in each of 64 t_1 increments at a ^{1}H frequency of 600 MHz. The 4′-^{13}C-Tyr... 19-^{13}C-retinal correlation can clearly be seen with DARR, but not with RFDR. This is similar to the results shown for AGG in Figure 3, and emphasizes the advantages of DARR for studies on membrane proteins.

These data provide the basis for studying metarhodopsin II, the active conformation of rhodopsin. Changes in cross peak intensity between the active and inactive states will give insight into the trajectory of the retinal upon isomerization relative to the assigned ^{13}C-labeled tyrosine residues.

Acknowledgements

This work was supported by a research grant to S.O.S. from the NIH (GM-41412), and NIH-NSF instrumentation grants (S10 RR13889 and DBI-9977553). We gratefully acknowledge the W.M. Keck Foundation for support of the NMR facilities in the Center of Structural Biology at Stony Brook.

References

Bennett, A.E., Rienstra, C.M., Auger, M., Lakshmi, K.V. and Griffin, R.G. (1995) *J. Chem. Phys.*, **103**, 6951–6958.

Bennett, A.E., Rienstra, C.M., Griffiths, J.M., Zhen, W.G., Lansbury, P.T. and Griffin, R.G. (1998) *J. Chem. Phys.*, **108**, 9463–9479.

Creemers, A.F.L., Kiihne, S., Bovee-Geurts, P.H.M., DeGrip, W.J., Lugtenburg, J. and de Groot, H.J.M. (2002) *Proc. Natl. Acad. Sci. USA*, **99**, 9101–9106.

Eilers, M., Reeves, P.J., Ying, W.W., Khorana, H.G. and Smith, S.O. (1999) *Proc. Natl. Acad. Sci. USA*, **96**, 487–492.

Farrens, D.L., Altenbach, C., Yang, K., Hubbell, W.L. and Khorana, H.G. (1996) *Science*, **274**, 768–770.

Griffiths, J.M., Bennett, A.E., Engelhard, M., Siebert, F., Raap, J., Lugtenburg, J., Herzfeld, J. and Griffin, R.G. (2000) *Biochemistry*, **39**, 362–371.

Gullion, T. and Schaefer, J. (1989) In *Advances in Magnetic Resonance, Vol. 13; Conference on 'High Resolution NMR in Solids', January 19–21, 1989*, Warren, W.S. (Ed.), pp. 57–84, Academic Press, Inc., San Diego, CA, London, UK.

Han, M., Lin, S.W., Smith, S.O. and Sakmar, T.P. (1996) *J. Biol. Chem.*, **271**, 32330–32336.

Jager, F., Fahmy, K., Sakmar, T.P. and Siebert, F. (1994) *Biochemistry*, **33**, 10878–10882.

Menon, S.T., Han, M. and Sakmar, T.P. (2001) *Physiol. Rev.*, **81**, 1659–1688.

Nakayama, T.A. and Khorana, H.G. (1991) *J. Biol. Chem.*, **266**, 4269–4275.

Okada, T., Fujiyoshi, Y., Silow, M., Navarro, J., Landau, E.M. and Shichida, Y. (2002) *Proc. Natl. Acad. Sci. USA*, **99**, 5982–5987.

Palczewski, K., Kumasaka, T., Hori, T., Behnke, C.A., Motoshima, H., Fox, B.A., Le Trong, I., Teller, D.C., Okada, T., Stenkamp, R.E., Yamamoto, M. and Miyano, M. (2000) *Science*, **289**, 739–745.

Peersen, O.B., Wu, X. and Smith, S.O. (1994) *J. Magn. Reson.*, **106**, 127–131.

Raleigh, D.P., Levitt, M.H. and Griffin, R.G. (1988) *Chem. Phys. Lett.*, **146**, 71–76.

Reeves, P.J., Kim, M.-J. and Khorana, H.G. (2002) *Proc. Natl. Acad. Sci. USA*, **99**, 3413–3418.

Reeves, P.J., Klein-Seetharaman, J., Getmanova, E.V., Eilers, M., Loewen, M.C., Smith, S.O. and Khorana, H.G. (1999) *Biochem. Soc. Trans.*, **27**, 950–955.

Robinson, P.R., Cohen, G.B., Zhukovsky, E.A. and Oprian, D.D. (1992) *Neuron*, **9**, 719–725.

Schmidt-Rohr, K. and Spiess, H.W. (1994) *Multidimensional Solid-State NMR and Polymers*, Academic Press, London.

Smith, S.O., Palings, I., Miley, M.E., Courtin, J., de Groot, H., Lugtenburg, J., Mathies, R.A. and Griffin, R.G. (1990) *Biochemistry*, **29**, 8158–8164.

Sodickson, D.K., Levitt, M.H., Vega, S. and Griffin, R.G. (1993) *J. Chem. Phys.*, **98**, 6742–6748.

Subramanian, E. and Lalitha, V. (1983) *Biopolymers*, **22**, 833–838.

Takegoshi, K., Nakamura, S. and Terao, T. (2001) *Chem. Phys. Lett.*, **344**, 631–637.

Takegoshi, K., Nakamura, S. and Terao, T. (2003) *J. Chem. Phys.*, **118**, 2325–2341.